View metadata, citation and similar papers at core.ac.uk

brought to you by CORE

provided by Elsevier - Publisher Connector

Available online at www.sciencedirect.com

SciVerse ScienceDirect

Physics Procedia 32 (2012) 139 – 143

Physics Procedia

18th International Vacuum Congress (IVC-18)

Microstructural and Electron-emission Characteristics of Nb-Si-N Films in Surface-conduction Electron-emitter Display

Huiyan Wu[a], Jianfeng Wang[a], Zhongxiao Song[a,]*, Shengli Wu[b], Yanhuai Li[a], Siliang Xiong[b], Kewei Xu[a,]*, Chunliang Liu[b]

[a]*State Key Laboratory for Mechanical Behavior of Materials, Xi'an Jiaotong University, Xi'an 710049, China*
[b]*Key Laboratory of Electronic physics and Devices of Ministry of Education, Xi'an Jiaotong University, Xi'an 710049, China*

Abstract

We proposed ternary nitride Nb-Si-N film as a promising surface-conduction electron emitter (SCE) in surface-conduction electron-emitter display (SED). Nb-Si-N films consisted of continuous NbN polycrystalline phase with $(Si_{3-x}Nb_{4x})N_4$ amorphous phase in NbN grain boundaries. After electroforming, serrated nanogaps were observed in Nb-Si-N SCE strips. The emission current of Nb-Si-N SCE array of 1×18 cells was 6.50 μA with anode voltage of 1.5 kV and device voltage of 22 V, indicating satisfying potential for display applications comparing with NbN SCEs. © 2012 Published by Elsevier B.V. Selection and/or peer review under responsibility of Chinese Vacuum Society (CVS). Open access under CC BY-NC-ND license.

PACS: 68.37.-d, 79.70.+q, 85.60.Pg,

Keywords: Surface conduction electron-emitter display; Nb-Si-N; microstructure; electroforming

1. Introduction

The surface-conduction electron-emitter display (SED) is considered as one of the most promising candidates for large-size flat-panel displays (FPDs) due to its simple structure, high image quality, wide viewing angle, quick response time, as well as low power consumption [1, 2]. As the key part of the SED, surface-conduction electron emitter (SCE) plays a crucial role in improving the performance of SED. SCEs are ultrafine particles conductive films with nanogaps produced through electroforming process [3]. As a result, the electron-emission characteristics of SCEs depend on the factors of both the emission material (work function of conductive films) and the emission regions (nanogaps' structure) [4]. Presently, some studies have been explored on electron-emission performance of SCEs based on electroforming process [5-9]. However, most of them were concerning conventional SCE material with low work function, such as Pd, C and Au. Other material systems, including some transition metal nitrides (such as NbN) which have proven ideal electron-emission material, have not been widely reported as SCEs yet [10, 11]. In addition, few researchers have provided more detail evidences about the microstructure of as-deposited SCE strips, and the impact of that on electron-emission characteristics after electroforming have not been illustrated

* Corresponding author. Tel.: +86-29-8231-0823; fax: +86-29-8266-3453.
E-mail address: zhongxiaosong@mail.xjtu.edu.cn, kwxu@mail.xjtu.edu.cn.

1875-3892 © 2012 Published by Elsevier B.V. Selection and/or peer review under responsibility of Chinese Vacuum Society (CVS).
Open access under CC BY-NC-ND license. doi:10.1016/j.phpro.2012.03.531

either. In this study, we proposed ternary nitride Nb-Si-N films as SCEs. Nb-Si-N films consisted of continuous NbN crystalline phase and amorphous phase introduced by the doping of Si. Owing to different microstructure from NbN, several serrated nanogaps formed successfully in Nb-Si-N SCE strips during electroforming. Uniform and stable electron-emission characteristics of the SCE array were observed. The results of Nb-Si-N SCEs were affirmative comparing with NbN SCEs, indicating an advisable SCE material system for display applications.

2. Experimental Details

NbN and Nb-Si-N films were both deposited on mirror-polished Si (100) wafers by reactive magnetron sputtering method. The base pressure of vacuum chamber was 5×10^{-5} Pa. The Nb (99.99%) target and Si (99.99%) target were co-sputtered in the mixture of argon and nitrogen (the flow rate of Ar/N_2: 4/1 sccm). During deposition, the sputtering power on Nb target was 100 W, when 0 W and 40 W were applied on Si target respectively for NbN and Nb-Si-N films. The bias voltage applied on the substrates was -100 V, and the thickness of films was 160 nm.

Under the same depositing conditions, NbN and Nb-Si-N SCEs were prepared on soda-lime glass substrates with 1×18 cells of patterned electrodes by photolithography procedure. The electrodes of Ni/Cu/Ni multilayer films were deposited by magnetron sputtering. The total thickness of electrodes was 150 nm. Fig.1 schematically shows the electroforming and testing system for a cell of SCEs array. The SCE strip was 400×100 μm^2, and the gap between the two co-planar electrodes was 10 μm in width. Electroforming was accomplished applying a triangle pulse voltage between two electrodes. The pressure of the chamber was better than 3×10^{-4} Pa in this process. When testing the electron-emission characteristics after electroforming, a stable high voltage (V_a) of 1.5 kV was applied between the anode and electrode. With a certain device voltage (V_f) between two electrodes, the emitter emission current (I_e) were measured by ampere meter.

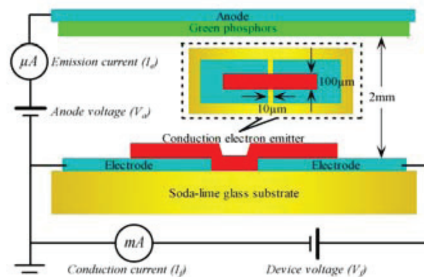

Fig. 1 Cross-sectional schematic diagram of the electroforming and testing system for a cell of electron emitter array

3. Results and Discussions

The atomic concentrations of Nb and N determined by X-ray photoelectron spectroscopy (XPS) are respectively 39.6% and 60.4% in NbN films, and that of Nb, Si and N for Nb-Si-N films are 29.3%, 11.2% and 59.5%, respectively. The inset of Fig.2 (a) shows XPS spectra of core-level Nb 3d for NbN and Nb-Si-N films. Both of the Nb 3d spectrums could be resolved into two peaks at binding energy of 204.0 eV and 206.7 eV corresponding to the Nb $3d_{5/2}$ and Nb $3d_{3/2}$ of NbN respectively [12, 13]. Meanwhile, the core level Si 2p spectrum of Nb-Si-N films in Fig.2 (a) consists of single peak at binding energy of 102.0 eV, which is attributed to the formation of Si_3N_4 [14]. The XPS results demonstrate that both the Nb and Si are fully nitrided in the films.

The crystal structure of films was analyzed by high-resolution transmission electron microscope (HRTEM). The TEM dark-field image of Nb-Si-N films (left inset of Fig.2 (b)) reveals that Nb-Si-N films have a columnar-growth structure of polycrystallites. According to the corresponding selected area electron diffraction (SAED) pattern (right inset of Fig.2 (b)), these grains are proved NbN crystallites with a face-centered cubic structure. NbN grains are fine, and the mean grain size is approximately 10 nm. The HRTEM results indicate that as-deposited Nb-Si-N films are basically composed of the same NaCl-type polycrystalline phase as that of pure NbN films (images not shown).

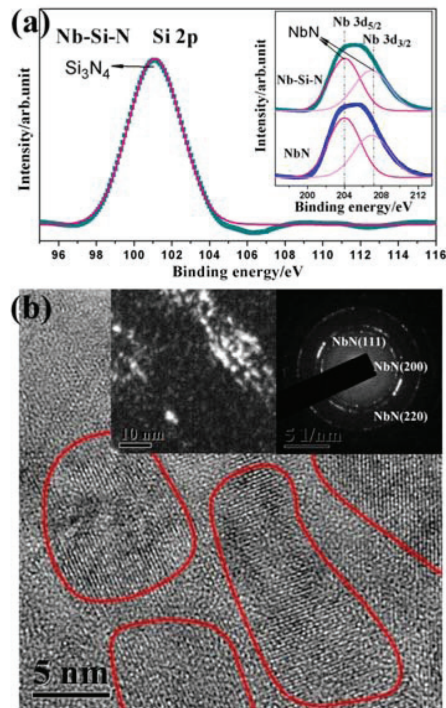

Fig. 2 Figure (a) is XPS spectra of core-level Si 2p for Nb-Si-N films, and the inset is XPS spectra of core-level Nb 3d for NbN and Nb-Si-N films. Figure (b) is HRTEM image of Nb-Si-N films. The left and right insets of (b) are TEM DF image and corresponding SAED pattern respectively.

In order to get a further understanding of Si existing state in Nb-Si-N films, energy dispersive spectroscopy (EDS) measurements were performed. Fig.3 shows HRTEM image of one grain boundary between two individual NbN grains in Nb-Si-N films. The upper inset is corresponding TEM bright-field image, and the lower two insets are typical point-EDS spectrums of the feature regions labeled A (including the grain boundary of approximately 1.2 nm wide) and B (adjacent NbN grain) in HRTEM image. Pronounced Si enrichment could be observed in grain boundary region. Based on the single scattering model [15, 16], the incident beam size d is 5.0 nm, and exit beam size D is 5.6 nm. Following an analysis methodology developed by Zhang et al [17], the interfacial excess of Si (Γ_{Si}) in NbN grain boundary is 25.8 nm^{-2}, which further proves Si predominant enrichment there. Researchers have reported a solid solution of Si atoms into NbN lattice when a small amount of Si is added [18, 19]. As an increasing doping of Si exceeding the solubility limit, extra Si atoms could segregate in some NbN grain boundaries, resulting in the formation of a $(Si_{3-x}Nb_{4x})N_4$ amorphous phase there. The XPS and EDS results reveal a two-phase structure in Nb-Si-N films at Si concentration of 11.2%, which consists of continuous NbN polycrystalline phase and $(Si_{3-x}Nb_{4x})N_4$ amorphous phase in NbN grain boundaries.

Fig. 4 (a) shows field-emission scanning electron microscopy (FESEM) image of NbN and Nb-Si-N SCEs after electroforming. On NbN SCE strip, a straight gap of hundreds of nanometers wide was formed in the step region connecting the electrodes and SCE strips. Meanwhile, on Nb-Si-N SCE strip, several serrated nanogaps were produced with width ranging from 30 nm to 80 nm. These nanogaps are randomly located all over the gap area between two electrodes. Fig.4 (b) shows the emitter emission current (I_e) of NbN and Nb-Si-N SCE array of 1×18 cells as a function of the device voltage (V_f) between two electrodes. The upper left inset of Fig.4 (b) is the corresponding Fowler-Nordheim (F-N) plot of I_e- V_f curve [20, 21]. The linear relationship between $Ln(I_e/V_f^2)$ and $(1/V_f)$ in the high device voltage region indicates that the electron conduction for NbN and Nb-Si-N both follow the Fowler-Nordheim field emission mechanism. The turn-on voltage of the SCE array, which is defined as the device voltage when the emission current begins to exhibit linear characteristic in the F-N plot, was about 15 V. For Nb-Si-N SCE array, a conduction current of 6.50 μA for 1×18 cells was observed at V_f of 22V and V_a of 1.5 kV, which is much larger than that for NbN SCEs. The lower right inset of Fig.4 (b) is the light spots of SCE array produced on the anode plate coated with green phosphors. In this figure, the Nb-Si-N SCE array could produce clearer light spots, indicating satisfying potential for display applications comparing with NbN SCEs.

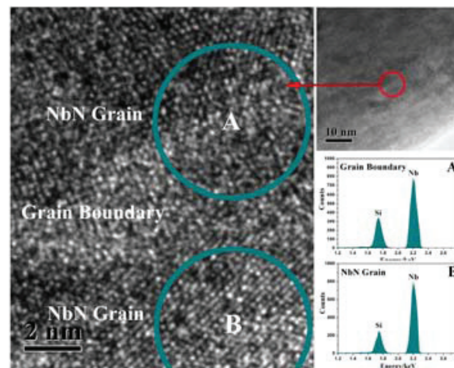

Fig. 3 HRTEM image of one grain boundary between individual NbN grains in Nb-Si-N films. The upper inset is corresponding TEM BF image, and the lower two insets are EDS patterns of the feature regions labeled A and B in HRTEM image.

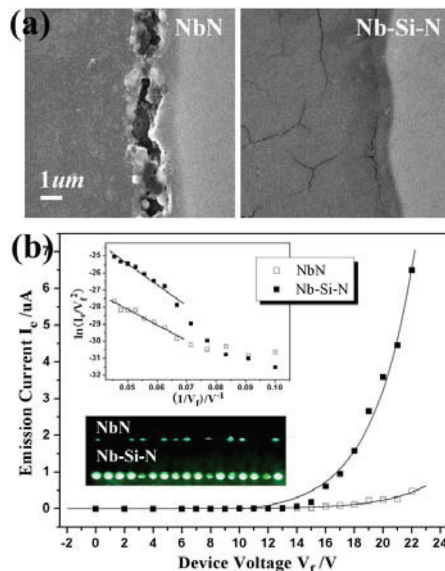

Fig. 4 Figure (a) is FESEM image of nanogaps formed in SCE strips. Figure (b) is emission current (I_e) of SCE array of 1×18 cells as a function of the device voltage (V_f) between two electrodes. The upper inset is corresponding Fowler-Nordheim (F-N) plot of I_e- V_f curve, and the lower inset is the light spots of SCE array produced on the anode plate coated with green phosphors.

As discussed above, the satisfying electron-emission characteristics depend on not only low work function of conductive films, but also favorable structure of nanogaps. In the case of Nb-Si-N SCEs, distributed serrated nanogaps should play an important role in improving the electron-emission performance. The formation of these nanogaps in Nb-Si-N SCE strips could be attributed to the new $(Si_{3-x}Nb_{4x})N_4$ amorphous phase introduced by appropriate doping of Si. On one hand, the sheet resistance of Nb-Si-N films is increased compared to NbN films owing to the existence of $(Si_{3-x}Nb_{4x})N_4$ amorphous phase in NbN grain boundaries [18]. With the same device voltage, a decreased conduction current could bring on weakened Joule heating, leading to an effective control on developing of thermal-stress in electroforming. On the other hand, $(Si_{3-x}Nb_{4x})N_4$ amorphous phase induces the decline of local mechanical properties in some wide NbN grain boundaries. As the thermal-stress accumulates gradually, the initiation of rupture occurs in these grain boundaries instead of the step region where stress concentration usually exists for NbN SCEs. Furthermore, relatively high concentration of rupture-initiated regions prevents these gaps become wider effectively, for thermal-stress could be released in time. During electroforming, amorphous phase gets rid of the formation of over sub-micro gaps by varying interrelated electrical and mechanical

properties. Based on this, we developed a two-phase structure for choosing advisable material systems in SCEs applications. Researchers extensively reported that ternary nitride (M-X-N) films consisting of a transition metal nitride (e.g. NbN, TiN, ZrN) films with addition of a third element X (e.g. Si, Ge) have similar microstructural, electrical and other characteristics [10, 22]. From this point of view, other ternary composite nitrides are under studying in our research group.

4. Conclusions

We proposed ternary nitride Nb-Si-N film as a promising SCE. The doping of Si introduced $(Si_{3-x}Nb_{4x})N_4$ amorphous phase into continuous NbN polycrystalline phase, which played a significant role in the formation of nanogaps in electroforming. Additionally, uniform and stable electron-emission characteristics of Nb-Si-N SCE array demonstrated satisfying potential for display applications.

5. Acknowledgements

This work was supported by Natural Basic Research Program of China (973 program) under Grant No. 2010CB31002, the National Natural Science Foundation of China (Grant No. 50871083) and Program for New Century Excellent Talents in University (Grant No. NCET-10-0641).

6. References

[1]. H.-Y. Lo, Y. Li, H.-Y. Chao, C.-H. Tsai, and F.-M. Pan, Nanotechnol. 184, 75708 (2007)
[2]. Y. Li, and H.-Y. Lo, J. Phy. D: Appl. Phys. 41, 085301 (2008)
[3]. I. Nomura, K. Sakai, E. Yamaguchi, M. Yamanobe, S. Ikeda, T. Hara, K. Hatanaka, and Y. Osada, Proc. IDW'96, 523 (1996)
[4]. Y. Li, and H.-Y. Lo, J. Nanosci. Nanotechnol. 9, 3271(2009)
[5]. T. Oguchi, E. Yamaguchi, K. Sasaki, K. Suzuki, S.Uzawa, and K. Hatanaka, SID Symp. Digest. 1929 (2005)
[6]. K. Yamamoto, T. Oguchi, K. Sakai, I. Nomura, S. Uzawa, k. Hatanaka, J. SID 14/1, 73 (2006)
[7]. Z. Wang, D. Li, B. Yao, J. Wang, Appl. Phys. Lett. 89,093503 (2006)
[8]. D. Zhu, D. Li, J. Wang, Chem. Phys. Lett. 447, 320 (2007)
[9]. C.-H. Tsai, F.-M. Pan, K.-J. Chen, C.-Y. Wei, M. Liu, and C.-N. Mo, Appl. Phys. Lett. 90, 163115 (2007)
[10]. M. Endo, H. Nakane, and H. Adachi, Appl. Surf. Sci. 94/95, 113 (1996)
[11]. Y. Gotoh, Y. Kashiwagi, M. Nagao, T. Kondo, H. Tsuji, and J. Ishikawa, J. Vac. Sci. Technol. B 19(4), 1373 (2001)
[12]. K.S. Havey, J.S. Zabinski, and S.D. Walck, Thin Solid Films 303, 238 (1997)
[13]. J.J. Jeong, and C.M. Lee, Appl. Surf. Sci. 214, 11 (2003)
[14]. P. Cova, S. Poulin, O. Grenier, and R.A. Masuta, J. Appl. Phys. 97, 073518 (2005)
[15]. J.R. Michael, and D.B. Williams, J. Microsc. 147, 289 (1987)
[16]. J.R. Michael, D.B Williams, C.F. Klein, and R. Ayer, J. Microsc. 160, 41 (1990)
[17]. X.F. Zhang, M.E. Sixta, and L.C. De Jonghe, J. Am. Ceram. Soc. 83, 2813 (2000)
[18]. C.S. Sandu, M. Benkahoul, R. Sanjines, and F. Levy, Surf. & Coat. Technol. 201, 2897 (2006)
[19]. Y. Dong, Y. Liu, J. Dai, and G. Li, Appl. Surf. Sci. 252, 5215 (2006)
[20]. R.H. Fowler, and L.W. Norfheim, Proc. R. Soc. London A 119, 173 (1928)
[21]. C.A. Spindt, I. Brodie, L. Humphrey, and E.R. Westerberg, J. Appl. Phys. 47, 5248 (1976)
[22]. C.S. Sandu, R. Sanjines, M. Benkahoul, F. Medjani, and F. Levy, Surf. & Coat. Technol. 201, 4083 (2006)